Supplementary Information for: EM Structure of human APC/C^{Cdh1}-EMI1 reveals multimodal mechanism E3 ligase shutdown

a

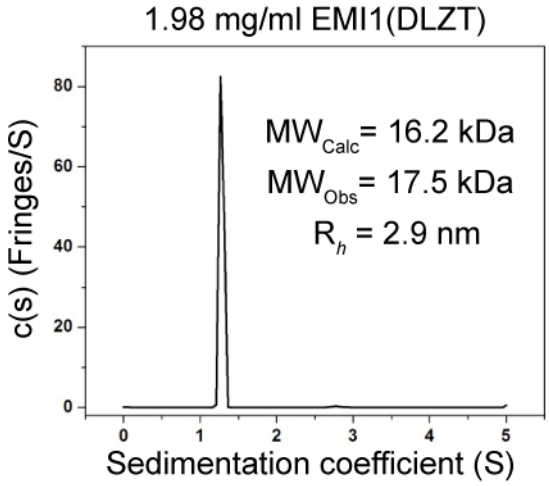

b

Sample	s_{20} (Svedberg)	$s^0_{20,w}$ (Svedberg)	f/f_0	M (kDa)	R_h (nm)
EMI1(DLZT) 1.98 mg/ml	1.28	1.38	1.85 (1.72)	17.5	2.93
EMI1(DLZT) 0.68 mg/ml	1.30	1.38	1.73 (1.72)	16.2	2.89

Supplemental Figure 1. Analytical Ultracentrifugation (AUC) of EMI1^{DLZT}.
AUC experiments were carried out in a ProteomeLab XL-I analytical ultracentrifuge with a four-hole Beckman An-60 Ti rotor and cells containing sapphire windows and charcoal-filled Epon double-sector centerpieces (Beckman Coulter, Fullerton, CA). The density of the ultracentrifugation buffer, 50 mM Tris pH 7.6, 150 mM NaCl at 20 °C were measured with an Anton Paar density meter (Anton Paar USA, Ashland, VA). The loading volume of 400 µl was identical for the reference and sample chambers of the double-sector centerpiece. Following a 1 hour temperature equilibration at 20 °C at rest the rotor was accelerated to 60,000 rpm and fringe displacement data at time intervals of 1.0 min were collected with the Rayleigh interference system for 12 hours.
(a) Sedimentation velocity profiles (fringe displacement) were fitted to a continuous sedimentation coefficient distribution model *c(s)*. Experiments were conducted at loading protein concentrations of 1.98 (shown above) and 0.68 mg/ml (Figure 1g) in 50 mM Tris, pH 7.6, 150 mM NaCl at 20 °C and at a rotor speed of 60,000 rpm. The viscosity of the buffer was calculated from its composition and the partial specific volume at 20 °C as well as the molecular weight of the protein was calculated based on its amino acid composition using the software SEDNTERP[1]. Buffer eluant from the size-exclusion column was used as an optical reference. Data were analysed with SEDFIT software (www.analyticalultracentrifugation.com) using the model for continuous sedimentation coefficient distribution *c(s)* with deconvolution of diffusional effects[2,3].

(b) Table of best-fit values and estimates of the *c(s)* analysis of Emi1 in 50 mM Tris pH 7.6, 150 mM NaCl .

The sedimentation coefficient distribution *c(s)* was calculated with maximum entropy regularization at a confidence level of p = 0.68 and at a resolution of sedimentation coefficients of n = 100. The positions of the meniscus and bottom, as well as time-invariant and radial noises, were fitted. A two-dimensional size-shape distribution, c(*s, f/f$_0$*) (with the one dimension the *s*-distribution and the other the *f/f$_0$*-distribution) was also calculated with an equidistant *f/f$_0$*-grid of 0.1 steps that varies from 1.0 to 2.5, a linear *s*-grid from 0.1 to 5 S with 100 s-values, and Tikhonov-Phillips regularization at one standard deviation (4). The distributions were transformed to *c(m,f/f$_0$), c(s,f/f$_0$), c(s,M)* and *c(s,R)* distributions with *M* the molecular weight, *f/f$_0$* the frictional ratio, s the sedimentation coefficient and R the Stokes radius and plotted as contour plots. This analysis was with regularization. The dotted lines of the *c(s,M)* distribution plot indicate lines of constant *f/f$_0$* . The distributions are not normalized[4].

The sedimentation coefficient (*s$_{20}$*) was taken from the ordinate maximum of each peak in the best-fit *c(s)* distribution. Sedimentation coefficient is a measure of the size and shape of a protein in a solution with a specific density and viscosity at a specific temperature. The $s^0_{20,w}$ -values (standard conditions of 20 °C, water as solvent, zero protein concentration), unit in Svedberg, represent converted *s*-values of the *c(s)* data. Best-fit weight-average anhydrous frictional ratio (*f/f$_0$)* and ratio was calculated with SENTERP and standard $s^0_{20,w}$–values in parenthesis. The molar mass values taken from the ordinate maximum of each peak in the best-fit *c(M)* distribution was calculated according to the method of Schuck[2]. For reference, the theoretical molecular weight is 16,175 Da.

The *c(s)* analysis of the sedimentation velocity data shows the presence of a single sedimenting species with a molecular weight for the low concentration sample to be 16,200 Da (very close to the theoretical molecular mass of 16,175 Da for Emi1) and a *f/f$_0$* value of 1.73. For the high concentration sample (1.98 g/l) a mass of 17,500 Da with a *f/f$_0$* value of 1.85 was calculated. The best-fit weight-average anhydrous frictional ratio $(f/f_0)_w$ of 1.73 for the 0.68 mg/ml sample, (close to the 1.72 value calculated with the standard $s^0_{20,w}$–value) indicates that the molecular shape of Emi1 is very elongated and extended. There may be some folding present in Emi1 because typical values for the hydrated frictional ratios range between 1.3 for nearly globular hydrated proteins to 2.0 for very elongated or glycosylated proteins[3].

The hydrodynamic radius of the protein was calculated using the software SEDFIT (www.analyticalultracentrifugation.com).

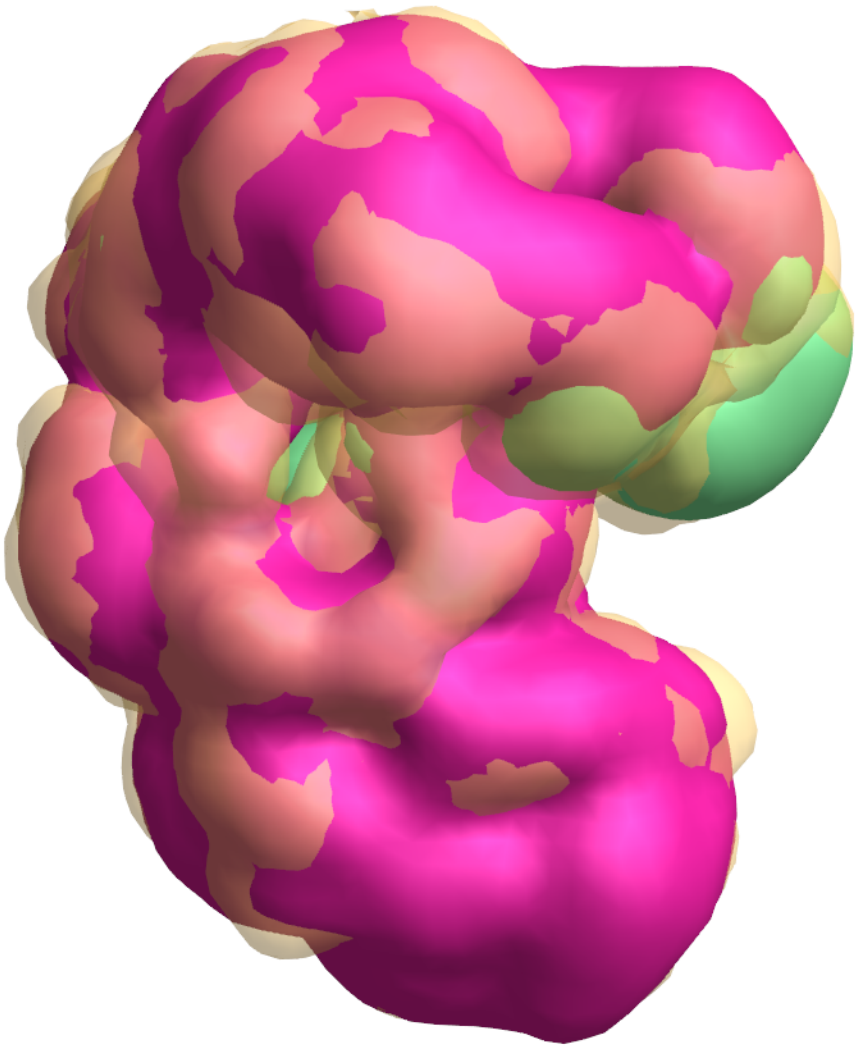

Supplemental Figure 2. Negative stain EM reconstructions.
(a) 3-dimensional PDF showing superposition of negative stain EM reconstructions of APC/C^{CDH1}-EMI1-SKP1 (yellow, transparent) with prior structure of human APC/C^{CDH1} (magenta, solid)[5]. The difference map shown in green reveals the location of EMI1-SKP1 and structural changes propagated throughout the APC/C^{CDH1} complex. Use of a mouse to rotate the 3D PDF allows visualization of the entire EM map.

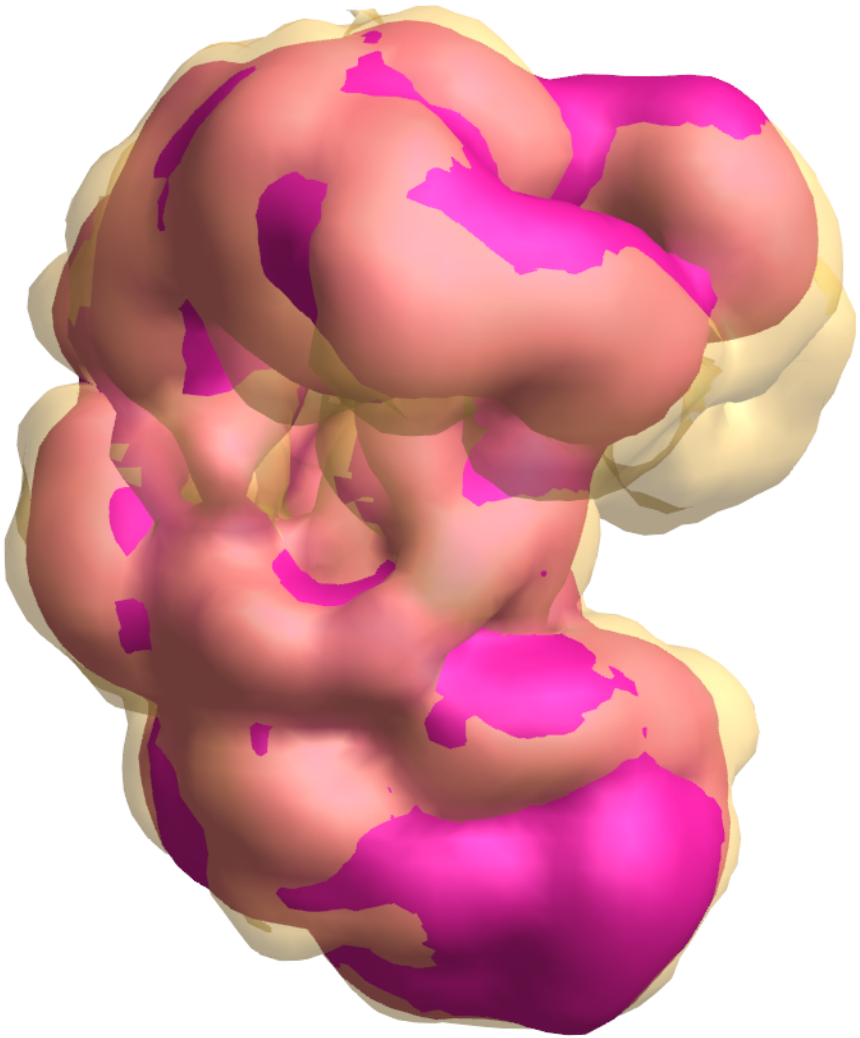

(b) 3D PDF showing superposition of negative stain EM reconstructions of APC/C^{CDH1}-EMI1-SKP1 (yellow, transparent) with prior structure of human APC/C^{CDH1} (magenta, solid)[5].

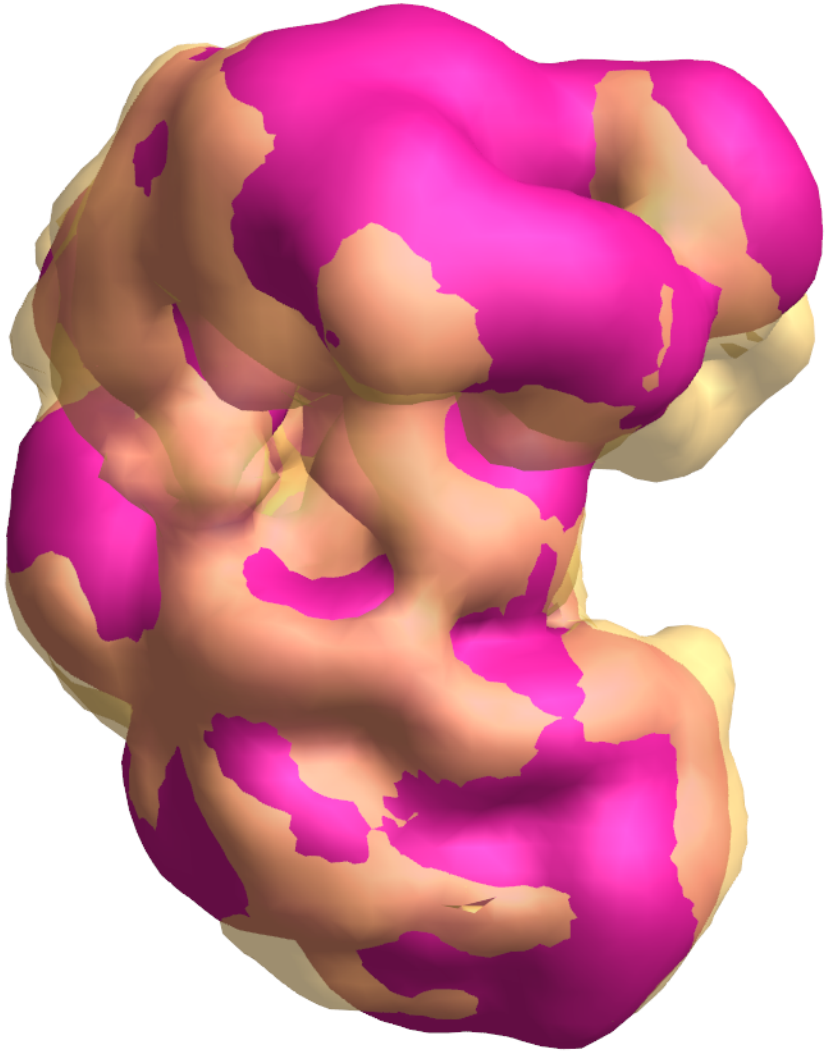

(c) 3D PDF showing superposition of negative stain EM reconstructions of APC/C^{CDH1}-EMI1^{DLZT} (yellow, transparent) with prior structure of human APC/C^{CDH1} (magenta, solid)[5].

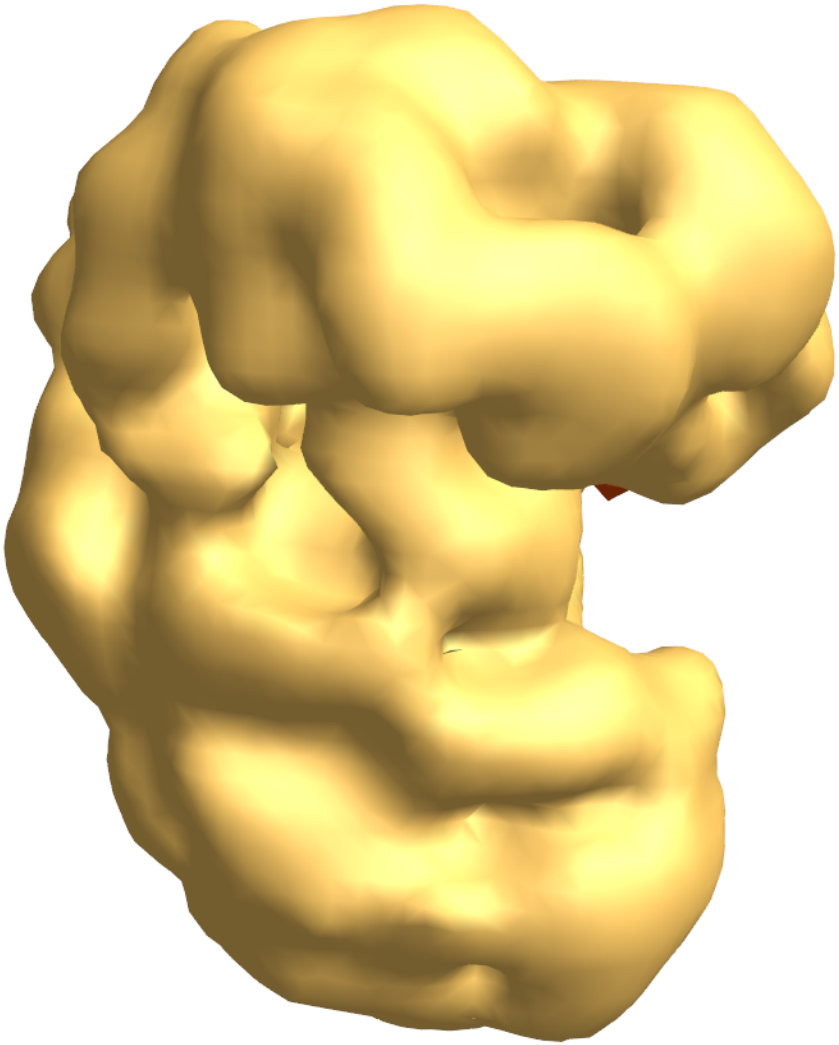

(d) 3D PDF illustrating EMI1 N-terminal domain localization. The main density not present in APC/C^{CDH1}-EMI1^{DLZT} compared to APC/C^{CDH1}-EMI1-SKP1 is shown in orange (from the APC/C^{CDH1}-EMI1-SKP1 - APC/C^{CDH1}-EMI1^{DLZT} difference map) on the EM reconstruction of APC/C^{CDH1}-EMI1^{DLZT}.

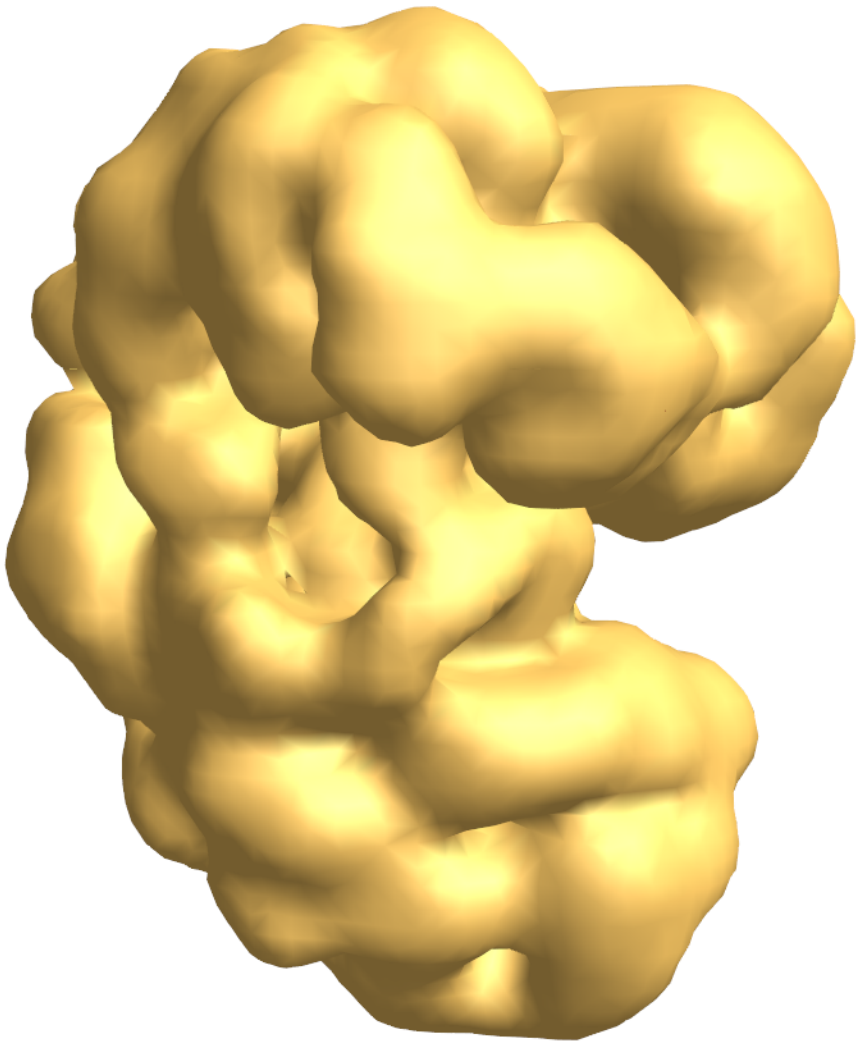

(e) 3D PDF illustrating MBP from the APC/C^{CDH1}-EMI1-MBPSKP1 complex. The main density not present in APC/C^{CDH1}-EMI1-SKP1 compared to APC/C^{CDH1}-EMI1-MBPSKP1 is shown in red (from the APC/C^{CDH1}-EMI1-MBPSKP1 - APC/C^{CDH1}-EMI1-SKP1 difference map) on the EM reconstruction of APC/C^{CDH1}-EMI1-SKP1.

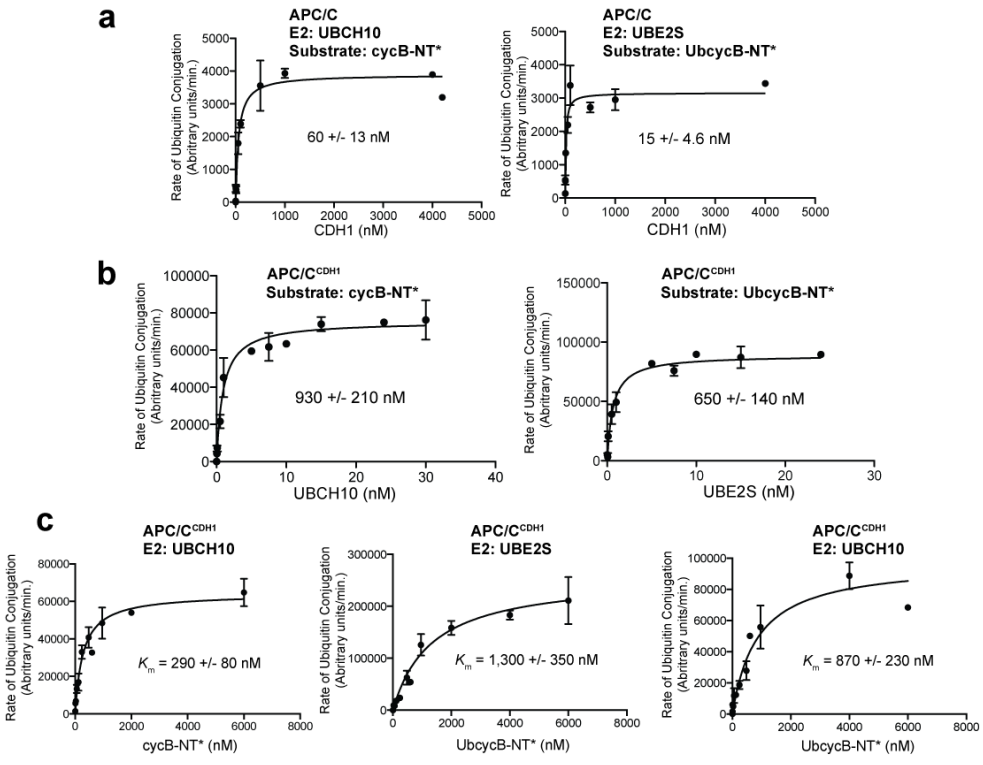

d

E2	Substrate	1/2 max CDH1 (nM)	$K_{m\ app}$ E2 (nM)	$K_{m\ app}$ Substrate (nM)
UBCH10	cycB-NT*	60 ± 13	930 ± 210	290 ± 80
UBCH10	UbcycB-NT*	ND	ND	1,300 ± 350
UBE2S	UbcycB-NT*	15 ± 4.6	650 ± 140	870 ± 230

ND = Not Determined

Supplemental Figure 3. Fitting of APC/C^{CDH1} kinetic data.

Error bars: SEM, n ≥ 3. The initial velocities were determined by performing APC/C^{CDH1}-mediated ubiquitination time courses with UBCH10 as the E2 and cycB-NT* as the substrate, UBCH10 as the E2 and UbcycB-NT* as the substrate, or UBE2S as the E2 and UbcycB-NT* as the substrate. Ubiquitinated products were quantitated and plotted versus time to determine the initial velocities (not shown). The initial velocities were then plotted against concentrations of CDH1, E2, or substrate. The CDH1 concentration was selected to achieve a fully occupied and homogeneous APC/C^{CDH1} population. An E2 concentration similar to the E2 $K_{m\ app}$ was chosen to determine the $K_{m\ app}$ of the substrates. If EMI1 competes with E2 or substrate but the E2 and substrate concentrations were higher than the $K_{m\ app}$, the identification of competitive inhibition would be more difficult. Data were fit to a hyperbolic curve by nonlinear regression to determine the ½ max and $K_{m\ app}$ values. Error was based on three independent measurements for each rate.

(a) Titrations of CDH1, with the APC/C, E2, and substrate concentrations fixed at 20 nM, 190 nM, and 200 nM, respectively.

(b) Titrations of E2s, with the APC/C, CDH1, and substrate concentrations fixed at 7 nM, 1 μM CDH1, and 200 nM, respectively.

(c) Titrations of substrate, with the APC/C, CDH1, UBCH10, and UBE2S concentrations fixed 2 nM, 1 μM, 900 nM and 600 nM, respectively.

(d) $K_{m\ app}$ values for E2s and substrates and ½ max CDH1 concentrations for the indicated APC/C^{CDH1}-dependent ubiquitination reactions.

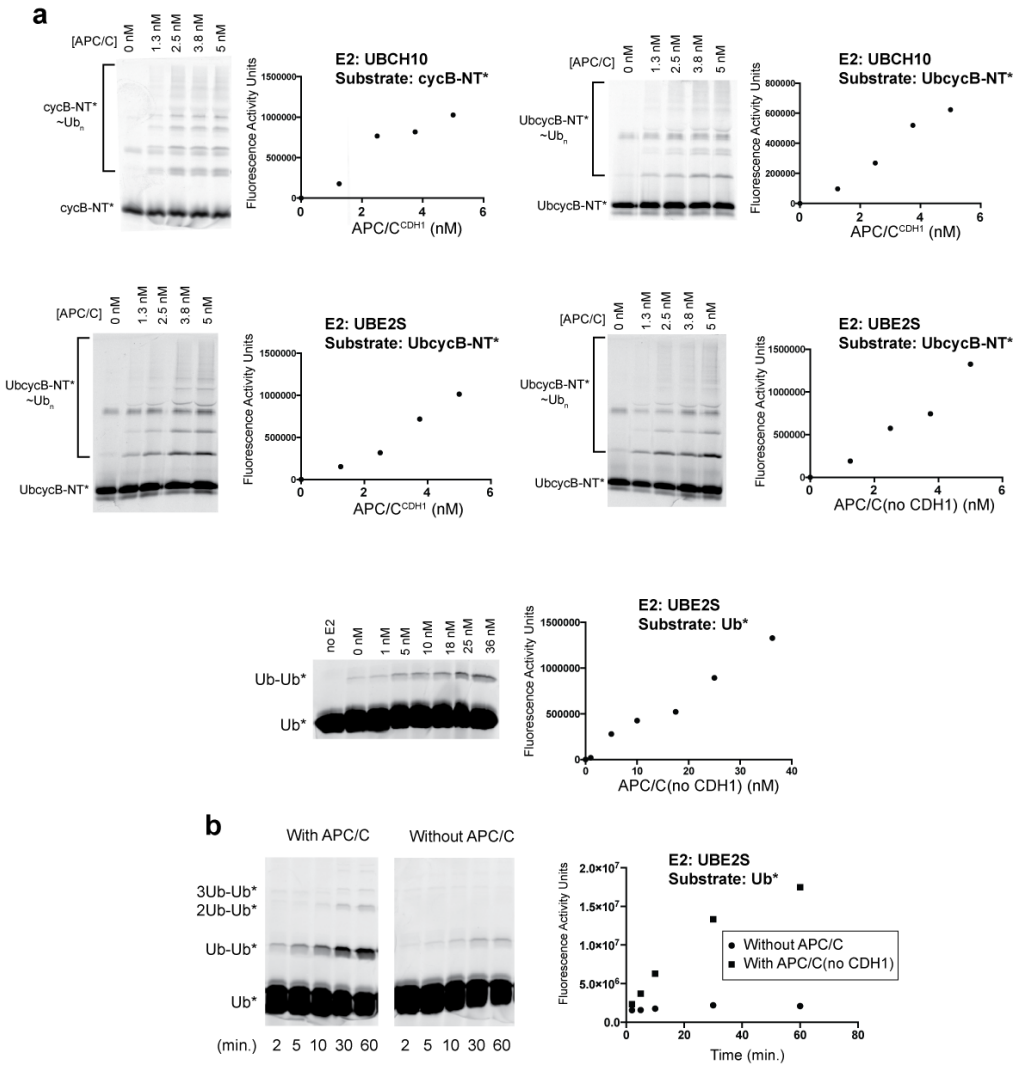

Supplemental Figure 4. Characterization of the ubiquitination reactions under initial velocity conditions used to determine the apparent inhibitory constants of EMI1 variants.

(a) Representative gels of APC/C-mediated ubiquitination reactions are shown using different E2/substrate combinations. The reactions were carried out at different APC/C concentrations while the concentrations of all other components were fixed as described in Supplementary Fig. 3c. The reactions were then quenched at their respective times and the ubiquitinated products were quantitated and plotted against the APC/C concentration. The linear relationship between the APC/C concentration and ubiquitinated product formation for each E2 and substrate combination suggest that the reactions are under initial velocity conditions.

(b) A time-course of the CDH1, D-box substrate-independent Ub chain formation assay is shown to demonstrate the dependence of UBE2S activity on APC/C concentration. In this assay, a fluorescent Ub* that cannot be carried through the E1-E2-E3 cascade was used as a Ub acceptor in APC/C- and UBE2S-dependent Ub chain formation assays.

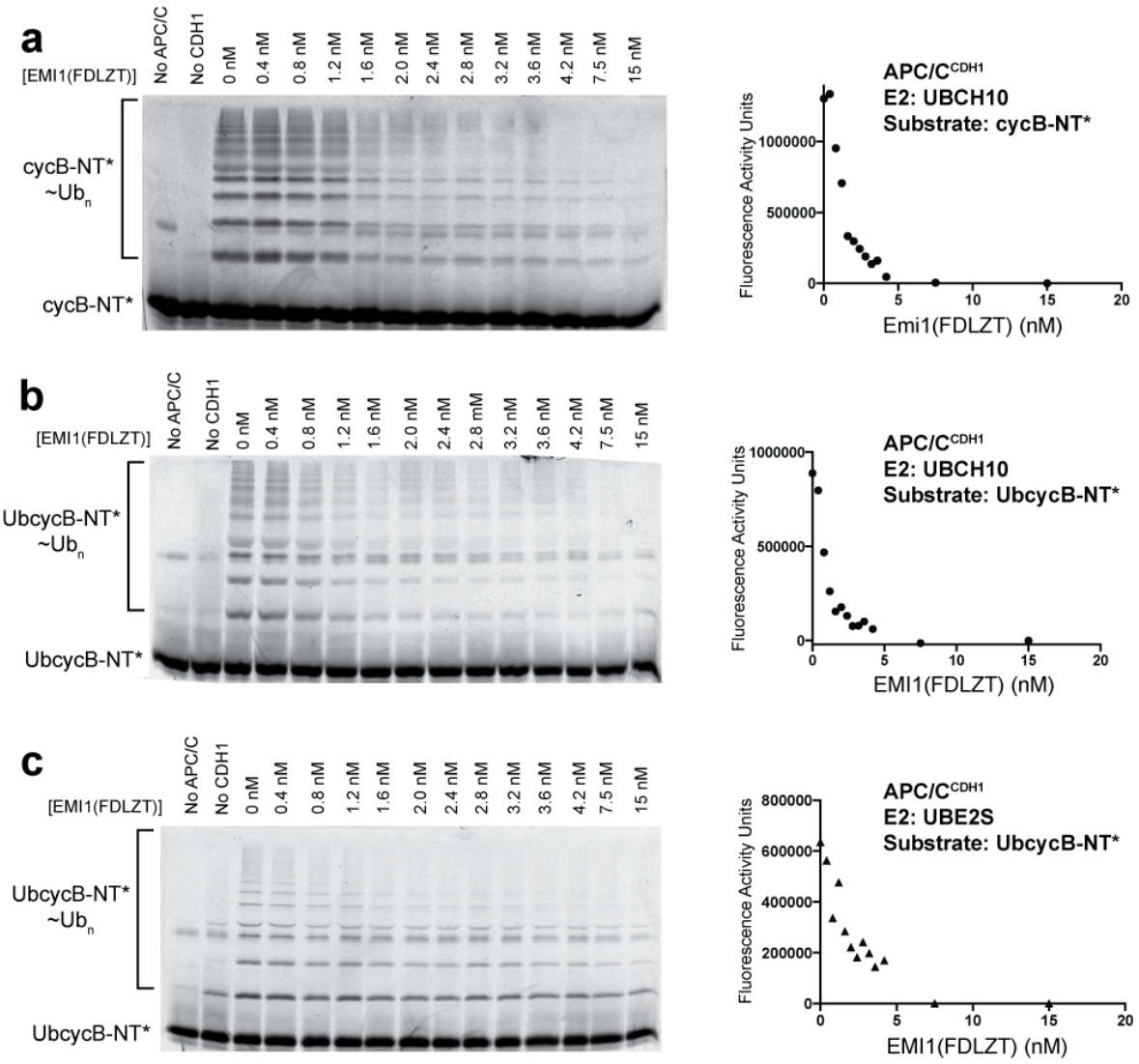
a
[EMI1(FDLZT)]
No APC/C
No CDH1
0 nM
0.4 nM
0.8 nM
1.2 nM
1.6 nM
2.0 nM
2.4 nM
2.8 nM
3.2 nM
3.6 nM
4.2 nM
7.5 nM
15 nM
cycB-NT* ~Ub$_n$
cycB-NT*
APC/C^{CDH1}
E2: UBCH10
Substrate: cycB-NT*
Fluorescence Activity Units
Emi1(FDLZT) (nM)
b
UbcycB-NT* ~Ub$_n$
UbcycB-NT*
EMI1(FDLZT) (nM)
c
E2: UBE2S
d
$$E_{free} = [E_0] - \frac{[E_0] + [I_0] + K_i^{app} - \sqrt{([E_0] + [I_0] + K_i^{app})^2 - (4[E_0][I_0])}}{2}$$
Simulated Data
K_i = 2.5 nM
K_i = 1.0 nM
K_i = 0.5 nM
K_i = 0.05 nM
Normalized Activity
[I] (nM)

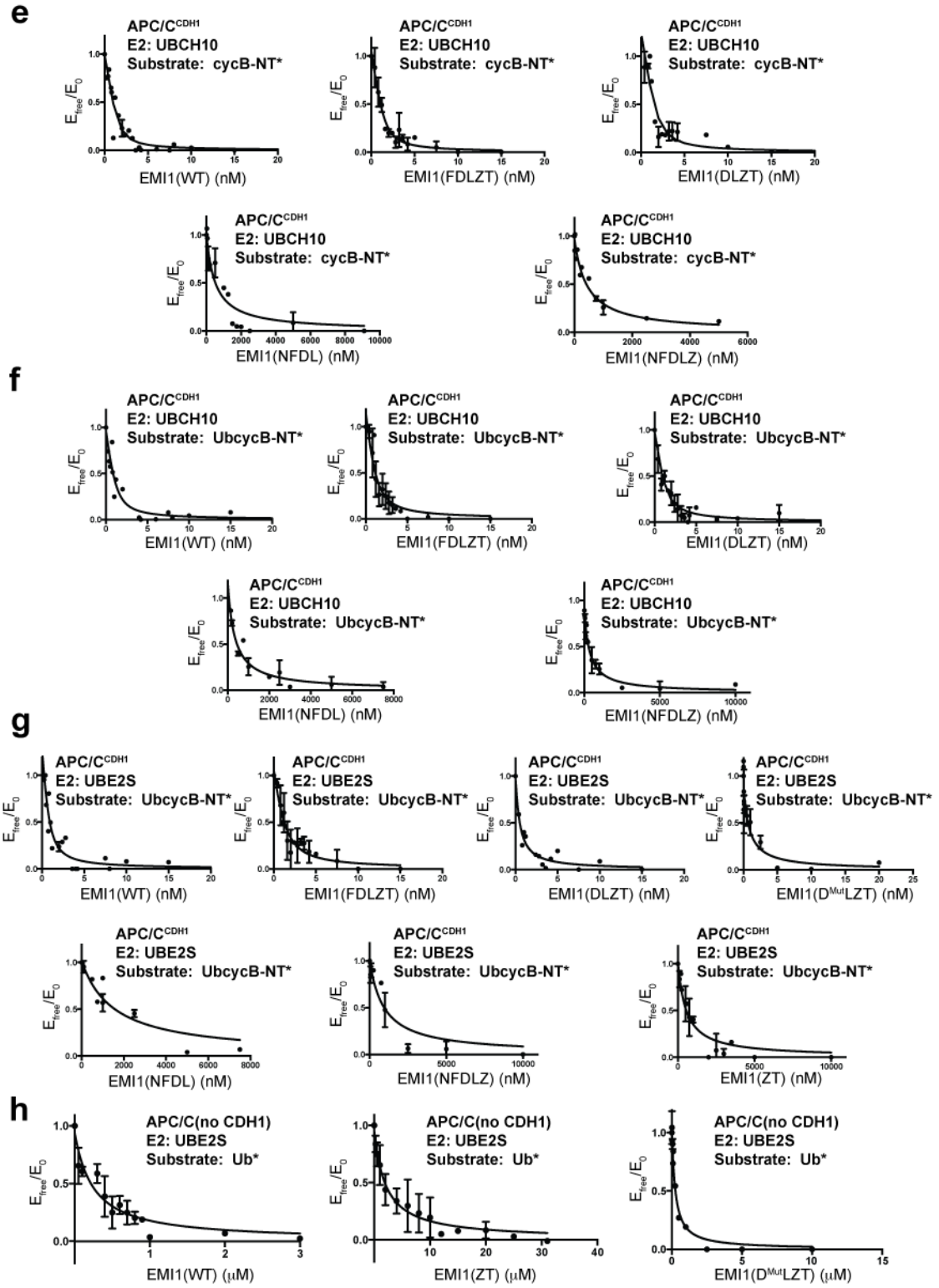
e
APC/C^{CDH1}
E2: UBCH10
Substrate: cycB-NT*
E_{free}/E_0
EMI1(WT) (nM)
EMI1(FDLZT) (nM)
EMI1(DLZT) (nM)
EMI1(NFDL) (nM)
EMI1(NFDLZ) (nM)
f
Substrate: UbcycB-NT*
g
E2: UBE2S
EMI1(D^{Mut}LZT) (nM)
EMI1(ZT) (nM)
h
APC/C(no CDH1)
Substrate: Ub*
EMI1(WT) (μM)
EMI1(ZT) (μM)
EMI1(D^{Mut}LZT) (μM)

Supplemental Figure 5. EMI1 is a tight binding inhibitor of both substrate ubiquitination and Ub chain forming activities of the APC/C^{CDH1}. Error bars: SEM, n ≥ 3. Representative gels showing concentration dependence of EMI1^{FDLZT}–SKP1 for inhibiting APC/C^{CDH1}-mediated ubiquitination reactions using three different E2 and substrate combinations, **(a)** UBCH10 as the E2 and cycB-NT* as the substrate, **(b)** UBCH10 as the E2 and UbcycB-NT* as the substrate, **(c)** UBE2S as the E2 and UbcycB-NT* as the substrate. The APC/C, CDH1, UBCH10, and UBE2S concentrations were fixed at 4 nM, 1 μM, 900 nM and 600nM, respectively. As shown in Supplementary Fig. 4, these reactions are under initial velocity conditions and therefore, the enzyme activity is sensitive to EMI1 inhibition. The ubiquitinated products were quantitated and plotted against EMI1^{FDLZT} concentration. The change in APC/C^{CDH1}-mediated ubiquitination by such subtle changes in EMI1 concentration around the APC/C concentration demonstrates the tight binding nature of EMI1. **(d)** The Morrison equation is a quadratic function for tight binding inhibitors that takes into account the depletion of E (Enzyme) and I (Inhibitor) upon the formation of the EI complex[6,7]. To assess the lower-limit for accurate $K_{i\ app}$ determination for EMI1 with this method, data were simulated for a range of theoretical K_i values using the tight-binding inhibitor/Morrison equation. Representative graphs with a range of theoretical K_i values are shown. The curves reveal the requirement to significantly detect enzyme activity at the stoichiometric point ("elbow") to accurately quantify $K_{i\ app}$ below 2.5 nM with 5 nM APC/C. However, tight binding versions of EMI1 almost completely deplete the active APC/C at the stoichiometric point, resulting in little remaining activity in this part of the titration. In these cases, instead of an equilibrium curve to determine the K_i, EMI1 is merely titrating the active enzyme concentration. The limited fits at the elbow region for our experiments thus set a lower limit of 2.5 nM for apparent K_i values that our assays can accurately measure. **(e-h)** Fitting of the EMI1-mediated inhibition of APC/C-dependent ubiquitination to determine apparent inhibitory constants reported in Table 1. Ubiquitinated products, quantified from gels similar to those shown in (a-c), plotted against EMI1 concentration and fit to Morrison tight binding equation (Eq.1, Methods).
(e) APC/C^{CDH1}- and UBCH10-dependent ubiquitination of cycB-NT*.
(f) APC/C^{CDH1}- and UBCH10-depdendent ubiquitination of UbcycB-NT*.
(g) APC/C^{CDH1}- and UBE2S-dependent ubiquitination of UbcycB-NT*.
(h) APC/C- and UBE2S-dependent ubiquitination of Ub*.

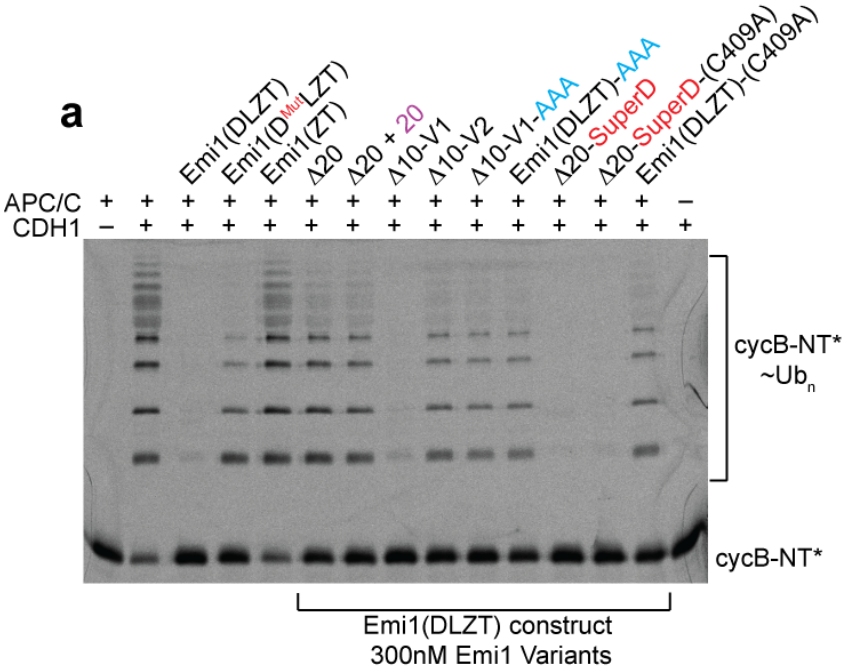

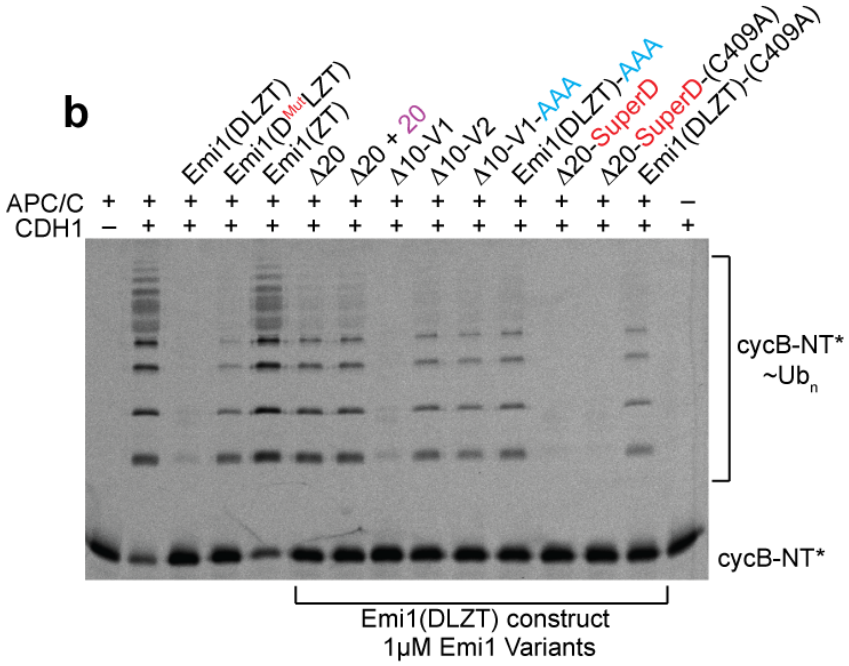

Supplemental Figure 6. Inhibition of APC/C^{CDH1} and UBCH10-mediated ubiquitination of cycB-NT* at extended reaction times. Data are shown for 300 nM (panel **a**) and 1 μM (panel **b**) of the indicated EMI1 variants described in Fig. 4.

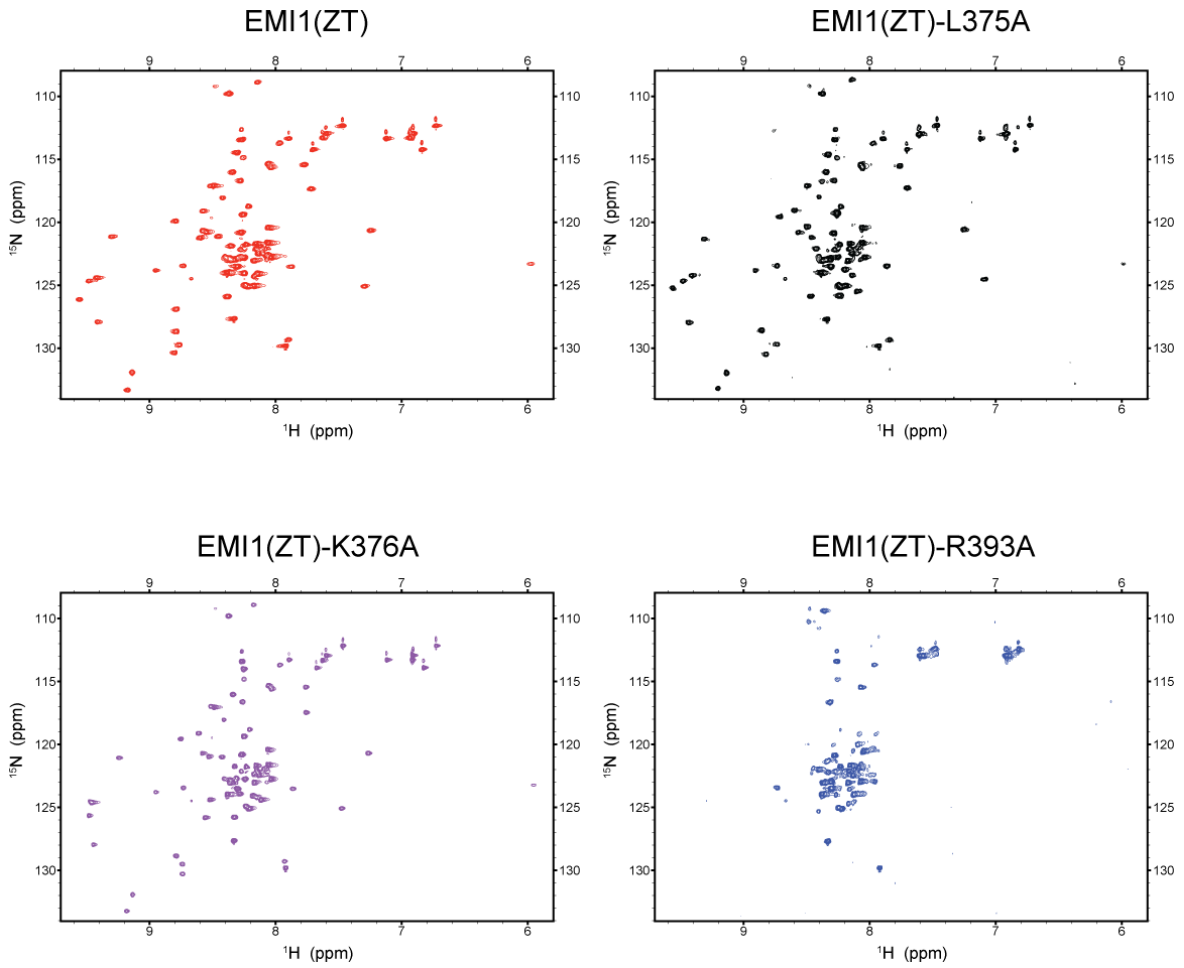

Supplemental Figure 7. ^{15}N-^{1}H HSQC spectra of selected EMI1^{ZT} variants. To compare the folding between variants and wild-type EMI1, the most defective alanine mutants (Fig. 5) were ^{15}N-labeled, purified, and examined by NMR. The L375A and K376A EMI1^{ZT} variants appear to be properly folded, whereas the R393A EMI1^{ZT} variant appears to be unfolded based on lack of dispersion for the observed resonances.

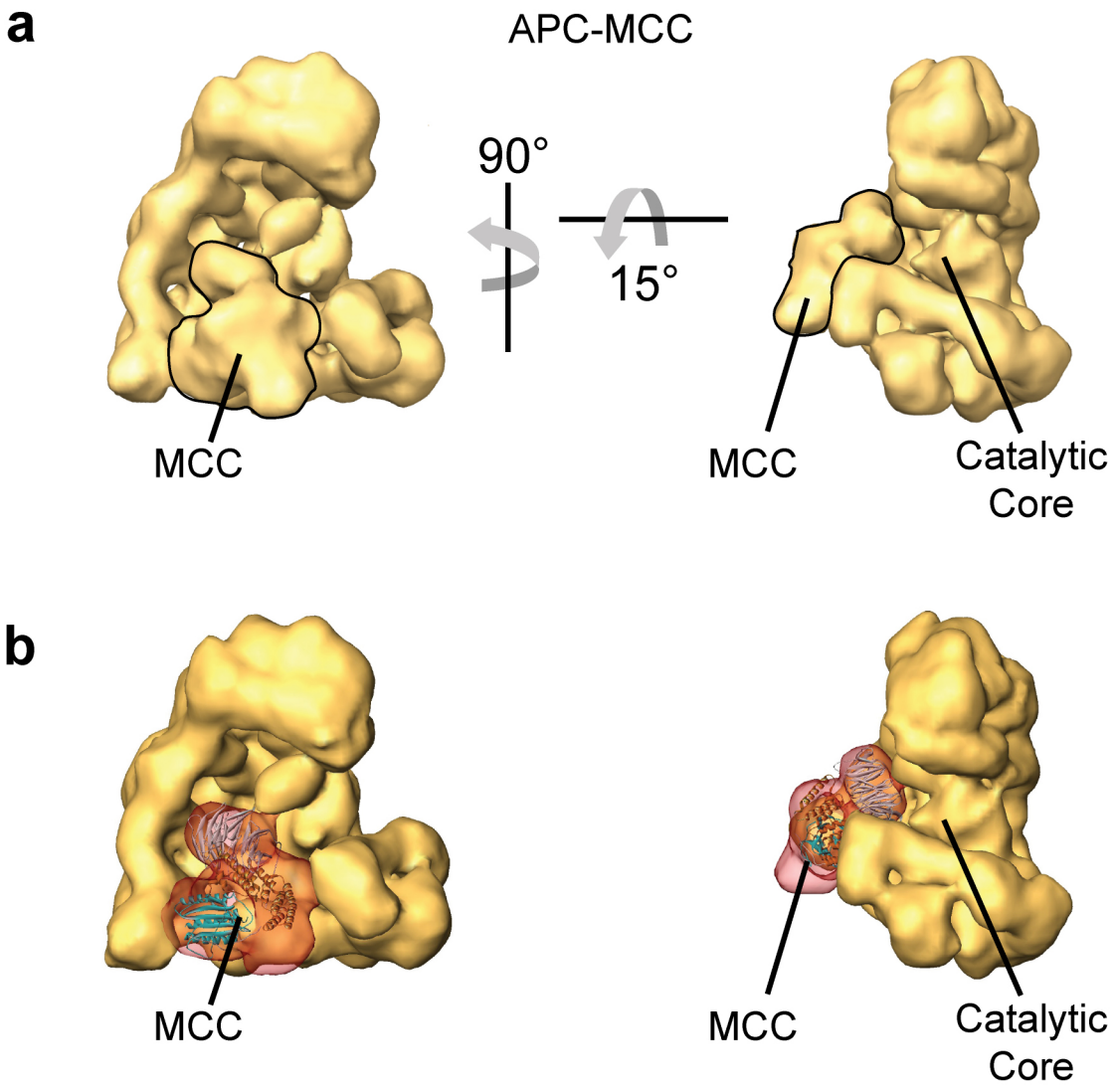

Supplementary Figure 8. Representation of prior structural data for APC/CMCC for comparison to APC/C^{CDH1}-EMI1^{DLZT}.
(a) Two views of human APC/C-MCC[8] with density attributed to MCC outlined for comparison to EMI1-bound complexes shown in Fig. 2. Note that MCC does not form the same contact to the catalytic core observed upon APC/C binding to EMI1.

(b) Similar views shown with transparent density for MCC over the crystal structure of a portion of *S. pombe* MCC[9].

Supplemental References

1. Laue, T.M., Shah, B.D., Ridgeway, T.M. & Pelletier, S.L. Computer-aided Interpretation of Analytical Sedimentation Data For Proteins. in *Analytical Centrifugation in Biochemistry and Polymer Science* (eds. Harding, S.E., Rowe, A.J. & Horton, J.C.) 90-125 (The Royal Society of Chemistry, Cambridge, UK, 1992).

2. Schuck, P. Size-distribution analysis of macromolecules by sedimentation velocity ultracentrifugation and lamm equation modeling. *Biophys J* 78, 1606-19 (2000).

3. Brown, P.H., Balbo, A. & Schuck, P. Characterizing protein-protein interactions by sedimentation velocity analytical ultracentrifugation. *Curr Protoc Immunol* Chapter 18, Unit 18 15 (2008).

4. Brown, P.H. & Schuck, P. Macromolecular size-and-shape distributions by sedimentation velocity analytical ultracentrifugation. *Biophys J* 90, 4651-61 (2006).

5. Buschhorn, B.A. et al. Substrate binding on the APC/C occurs between the coactivator Cdh1 and the processivity factor Doc1. *Nat Struct Mol Biol* 18, 6-13 (2011).

6. Morrison, J.F. Kinetics of the reversible inhibition of enzyme-catalysed reactions by tight-binding inhibitors. *Biochim Biophys Acta* 185, 269-86 (1969).

7. Copeland, R.A. Evaluation of enzyme inhibitors in drug discovery. A guide for medicinal chemists and pharmacologists. *Methods Biochem Anal* 46, 1-265 (2005).

8. Herzog, F. et al. Structure of the anaphase-promoting complex/cyclosome interacting with a mitotic checkpoint complex. *Science* 323, 1477-81 (2009).

9. Chao, W.C., Kulkarni, K., Zhang, Z., Kong, E.H. & Barford, D. Structure of the mitotic checkpoint complex. *Nature* 484, 208-13 (2012).